Desalination and Water Treatment
www.deswater.com

doi: 10.1080/19443994.2013.818924

52 (2014) 6822–6831
October

Taylor & Francis
Taylor & Francis Group

Analyzing pump impeller for performance evaluation using RSM and CFD

M. Nataraj[a], R. Ragoth Singh[b,*]

[a]*Department of Mechanical Engineering, Government College of Technology, Coimbatore, India*
[b]*Department of Mechanical Engineering, Karpagam College of Engineering, Coimbatore, India*
Email: ragothsingh@rediffmail.com

Received 10 January 2013; Accepted 14 June 2013

ABSTRACT

This paper illustrates the improvement in the performance of a centrifugal pump by modifying impeller design specifications via response surface methodology (RSM) complemented with computational fluid dynamics (CFD) simulations. Impeller geometry is varied at the best efficiency point (BEP) to get hold of the performance of the pump. The pump characteristics are evaluated by studying the impeller eye diameter, vane exit angle, and width of impeller blade at exit. Different pump models were analyzed by modifying the critical design parameters via central composite design. CFD analysis is carried out for the developed models to predict the performance of the pump and experimental studies were conducted to validate the CFD. Conformation experiments were performed to verify the optimal design specifications. Good agreements between the predicted and actual values of responses have been observed. The RSM- and CFD-based optimized impeller parameters yield an increase in total head from 39.66 m to 41.72 m and the power consumption is minimized from 432.17 W to 366.95 W at BEP.

Keywords: Centrifugal pump; Impeller; Central composite design; Response surface methodology; Computational fluid dynamics

1. Introduction

Centrifugal pump is a useful rotordynamic machine in fluid flow arena as it is extensively used in irrigation, industry, large plants, domestic, and river water pumping systems. These pumps are used at places where the requirements of head and discharge are moderate. The operational characteristics of the pump such as power, head, and flow rate mainly depend on impeller geometry. Modifications in impeller geometry have direct influence on recirculation, cavitations, and pressure pulsations in flow field and also increase the power requirement. The pump manufacturer's profit may reduce if prototypes are tested because of the trial-and-error testing methods. Many research studies have been taken up in pump industries using computational fluid dynamics (CFD) to improve the performance. This paper discusses the response surface methodology (RSM)-based design optimization of a centrifugal pump and the results were analyzed using CFD fluent software. Parameters such as impeller eye diameter, vane exit angle, and width of the blade at exit were optimized using RSM. Fig. 1 illustrates the methodology adopted in this research study to achieve the objective.

*Corresponding author.

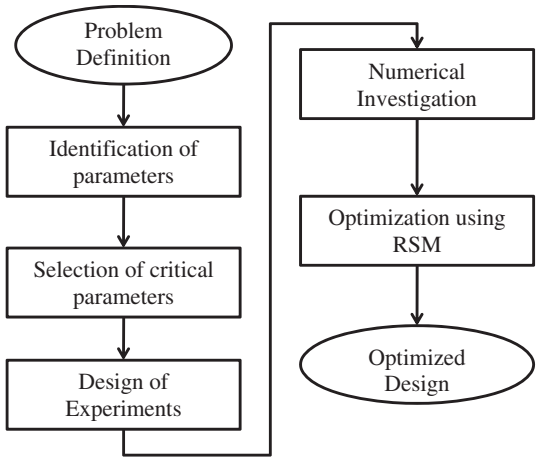

Fig. 1. Research methodology.

Hydrodynamic and optimization analysis were performed numerically using shear stress transport turbulence model with four design variables on a radial basis neural network model for a vane diffuser in a mixed-flow pump [1]. Shojaeefard et al. carried out an experimental study for performance improvement of centrifugal pump by modifying the geometric characteristics using CFD for viscous fluid [2]. Sun-Sheng Yang et al. predicted the performance of the pump working as turbine numerically, along with experimental and theoretical analysis [3]. Flow simulations were performed by varying the number of blades of the impeller using turbulence models [4]. CFD analysis was performed on the unsteady flow behavior near the tongue region of a centrifugal pump for three-dimensional unsteady flow with reference to grid size, time step size, and turbulence model [5]. The performance of the pump is numerically optimized on a two-dimensional (2D) centrifugal pump impeller to find the impeller geometry for maximizing the pump efficiency by varying the design variables of blade angles at the leading and the trailing edge [6]. Centrifugal pump model were studied by numerical simulations, and performance tests were conducted to study the hydraulic properties of the ultra-low specific-speed centrifugal pump [7]. A CFD code with 2D cascade model was developed to predict the cavitation behavior around the impeller blades of the impeller in a centrifugal pump [8]. Key parameters in the design process that are likely to have an effect on the head, discharge, and power variation in the pump had been discussed by many researchers [9–16]. Multiobjective optimization of the semi-open impeller in a centrifugal pump was done using numerical analysis [17]. A design methodology in the optimization of photo catalytic degradation of azo dye using RSM and the experiments were carried out in central composite design (CCD) consisting of 20 experiments determined by the 2^3 full factorial designs with six axial points and six center points [18]. An approach was made for tuning the parameters of an artificial neural network using central composite design and genetic algorithm [19].

Table 1
The physical dimension of the impeller

Parameter	Dimension
Outer diameter of impeller	162 mm
Eye diameter of impeller	27 mm
Vane angle at inlet	19°
Vane angle at outlet	43°
Blade width	3.5 mm
Number of vanes	5
Number of splitter vanes	5

2. Numerical simulation

2.1. Geometry modeling

A domestic centrifugal pump was modeled at the duty flow condition of 0.8333 lps, head of 35 m, and speed of 2,800 rpm for a specific speed of 6 (rpm, m^3/s, m). The physical dimensions of the impeller (Table 1) for the pump were obtained from a South Indian pump manufacturer [20]. Fig. 2 shows the impeller model created using CATIA for the physical dimensions.

2.2. Steps and tools in CFD

CFD uses numerical methods to solve the fundamental nonlinear differential equations that describe

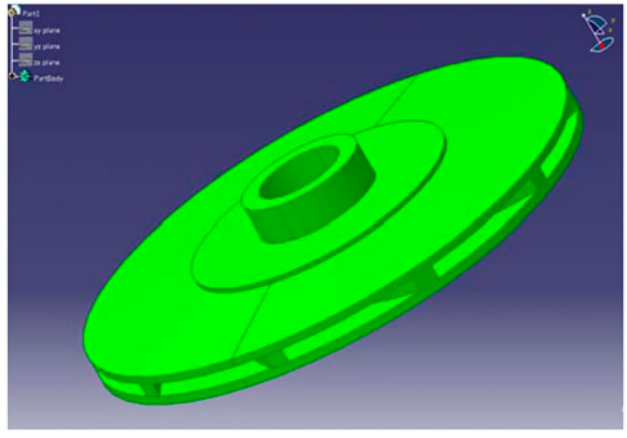

Fig. 2. Model of the impeller.

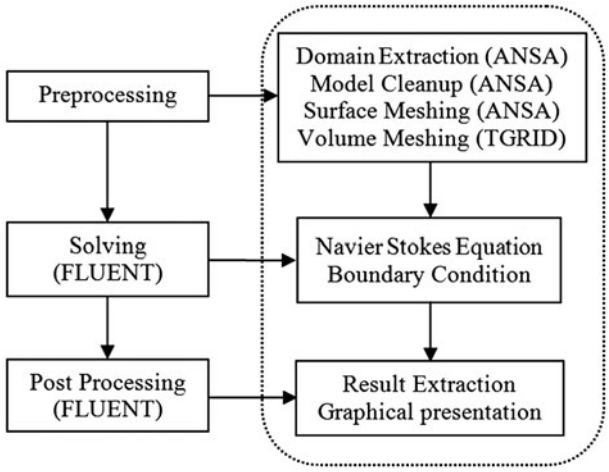

Fig. 3. Steps and tools involved in CFD.

fluid flow (Navier-Stokes and allied equations) for predefined geometries and boundary conditions. CFD is used to envisage the performance of the pump at various conditions. The flow characteristics such as pressure, volumetric flow, velocity, and temperature at each point can be obtained from CFD. The overall flow pattern and pressure distribution in the whole volume of flow can be obtained in the form of graphical representation for best understanding. The steps involved in CFD are shown in Fig. 3. The centrifugal impeller solid models were developed using CATIA and exported to a STEP file. The STEP files were then imported into ANSA, the mesh generator. In ANSA, the model construction and split were processed. The fluid volume was set for inlet and outlet in the impeller volume. The inlet and outlet flows were fully developed. Constant rotational speed is set for impeller volume and was fixed as a rotating reference frame. Successive numerical simulations were done to obtain the characteristics to predict the pressure developed and torque created by the fluid against rotation on the modified impeller geometry to predict its performance by giving its working conditions as input. The head and power were calculated from the CFD results as given in Table 3. Many assumptions such as number of elements, element types, turbulence model, etc. have to be made by trial and error for getting solution for the problem on hand; the assumptions that match with the CFD results and experimental results are chosen for further analyses.

2.3. Governing equations

Whatever be the flow pattern, whether it is compressible/incompressible, steady/unsteady, laminar/turbulent, the fluid behavior is governed by the fluid dynamics and the following physical laws are adopted [13].

Mass is conserved for the incompressible fluid at steady state as:

$$\frac{\partial}{\partial X_i}(u_i) = 0 \tag{1}$$

The following form of Navier–Stokes equation was used for the fluid analysis in the entire pump at the steady state:

$$\frac{\partial}{\partial X_j}(\rho u_i u_j) = \frac{\partial P}{\partial X_i} + \frac{\partial P}{\partial X_j}\left[\mu\left(\frac{\partial u_i}{\partial X_j} + \frac{\partial u_j}{\partial X_i} - \frac{2}{3}\delta_{ij}\right)\right] + \frac{\partial}{\partial X_j}\left[\mu_t\left(\frac{\partial u_i}{\partial X_j} + \frac{\partial u_j}{\partial X_i}\right) - \frac{2}{3}\left(pk + \mu_t\frac{\partial u_i}{\partial X_i}\delta_{ij}\right)\right] \tag{2}$$

where ρ, p, and u_i denote fluid density, mean static pressure, and fluid velocity, respectively.

2.4. Turbulence model: standard K-ε

The standard K–ε model, the most frequently used turbulence model in CFD codes was used in the simulation [14].

For turbulent kinetic energy K:

$$\frac{\partial}{\partial t}(\rho k) + \frac{\partial}{\partial x_i}(\rho k u_i) = \frac{\partial}{\partial x_j}\left[\left(\mu + \frac{\mu_t}{\sigma_k}\right)\frac{\partial k}{\partial x_j}\right] + G_k + G_b - Y_M + S_k - \rho\varepsilon \tag{3}$$

For dissipation ε:

$$\frac{\partial}{\partial t}(\rho\varepsilon) + \frac{\partial}{\partial x_i}(\rho\varepsilon u_i) = \frac{\partial}{\partial x_j}\left[\left(\mu + \frac{\mu_t}{\sigma_\varepsilon}\right)\frac{\partial \varepsilon}{\partial x_j}\right] + C_{1\varepsilon}\frac{\varepsilon}{K} \times (G_K + C_{3\varepsilon}G_b) - C_2\rho\frac{\varepsilon^2}{K} + S_\varepsilon \tag{4}$$

The default values for the constants in the above equations are $\mu_t = \rho v_t; v_t = c_\mu \frac{K^2}{\varepsilon}$ $C_{1\varepsilon} = 1.44; C_{2\varepsilon} = 1.92;$ $C_\mu = 0.9; \sigma_k = 1.0; \sigma_\varepsilon = 1.3.$

2.5. Grid and boundary conditions

The fluid flow path was extracted from 3D model of the pump in the preprocessing stage. Model cleanup process removes unwanted surfaces, corrects overlapping surfaces, and removes the clearance between them.

A total of 0.4 million triangular elements (Fig. 4) were used for creating surface mesh with skewness of

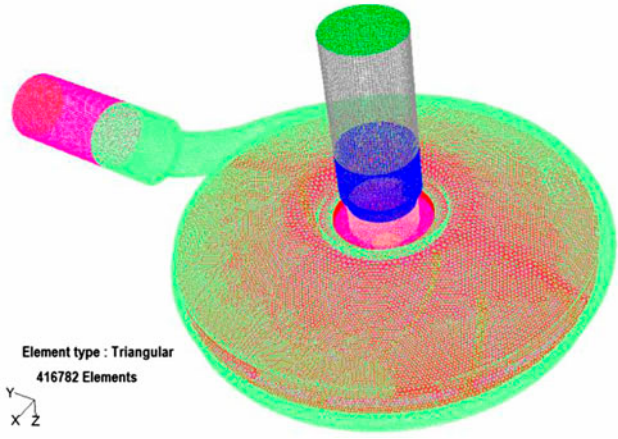

Fig. 4. Surface mesh.

0.6. Volume mesh was created from the surface mesh with 1.3 million tetrahedron elements with skewness of 0.75. Five grid refinements were performed for grid independence test. Virtual analyses have been carried out with 1.1–1.5 million volume mesh elements to predict the performance of the pump under the duty point condition. Minimum variations in volume flow rate were noticed after 1.3 million elements. For this reason, there could not be appreciable change in the flow rate even the mesh elements were increased thereafter.

3. Experimental design and analysis

Analysis has been carried out on the meshed volume to predict the performance of the pump under the following duty point conditions of volume flow rate of 0.8333 lps and rotational speed of 2800 rpm with boundary conditions (Fig. 5).

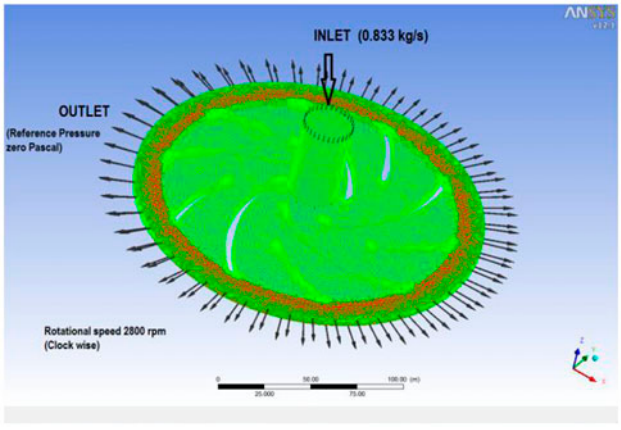

Fig. 5. Boundary conditions.

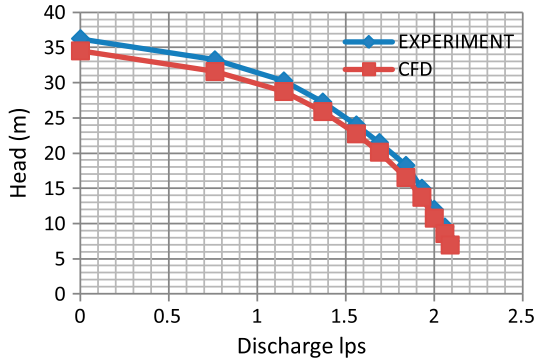

Fig. 6. Experimental and CFD performance curves.

CFD simulations performed using FLUENT for which the assumptions made are: (1) incompressible flow; (2) steady state flow but viscous fluid with the rotor zone treated as moving frame (rotating turbine wheel zone); and (3) smooth walls with no-slip boundary. Standard K–ε turbulence model and first-order discretization scheme have been chosen for analysis. The assumptions which match the results with the experimental performance curve were noted. Fig. 6 gives an idea about how the CFD results depart from the experimental results. The variation of 3.5–4.9% in CFD results when compared with experimental results with regard to head indicates that the analysis were in good agreement with each other.

3.1. Central composite design

The CCD-based RSM approach is the most efficient tool to identify the optimum parameters for centrifugal pump impeller. It can be naturally partitioned into two subsets of points; the first subset estimates linear and two-factor interaction effects while the second subset estimates curvature effects. The second subset need not process when analysis of the data from the first subset points indicates the absence of significant curvature effects. CCD approach is well matched with three factors and two levels (low and high); 20 runs were obtained as $2^n + 2n + 6$, where n is the number of factors ($n = 3$). Detailed analysis for control factors A (impeller eye diameter), B (vane exit angle), and C (width of the blade at exit) has been carried out to fix the lower and upper limits, and each variable was designated by low, middle, and high levels as −2, 0, and +2 and the factor levels and its range chosen are given in Table 2 [19,20].

The significant independent variables A, B, and C and the mathematical relationship of the response (Y) on these variables can be approximated by the second-degree polynomial equation by multiple regression technique.

Table 2
Factors with level

Factors	Level of value				
	−2	−1	0	1	2
A: Impeller eye diameter (mm)	25	26	27	28	29
B: Vane exit angle (°)	32	37.5	43	48.5	54
C: Blade width at exit (mm)	3.5	4	4.5	5	5.5

$$x_i = \frac{x_i - x_{io}}{\Delta x_i} \tag{5}$$

where x_i is the ith independent variable of the coded value, X_i the natural value of the ith independent variable, x_{io} the natural value of the ith independent variable at the center point, and Δx_i is the step change value.

$$Y = b_0 + \sum_{i=1}^{k} b_i x_i + \sum_{i=1}^{k} b_{ii} x_i^2 + \sum_{i=1}^{k-1} \sum_{j=2}^{k} b_{ij} x_i x_j + e \tag{6}$$

where Y is the predicted response; x_i and x_j are variables; b_0 is the constant coefficient; b_i, b_{ii}, and b_{ij} are interaction coefficients of linear, quadratic- and second-order terms, respectively; k is the number of factors studied; and e is the error [19,20]. The total numbers of experimental runs developed are indicated in Table 3.

3.2. RSM analysis

The CFD data were analyzed in RSM using the second-order polynomial equation for the responses using MINITAB software package [19]. The test is necessary to fit an adequate approximation model to the actual system. The regularity was entrenched by the linear, linear squares, linear interactions, or full quadratic fit of each experimental run of all residuals plots from observed and predicted data. The responses of observed and predicted values were fitted with 95% confidence for regression equations.

$$Y = b_0 + b_1 A + b_2 B + b_3 C + b_{11} A^2 + b_{22} B^2 + b_{33} C^2 + b_{12} AB + b_{13} AC + b_{23} BC \tag{7}$$

where Y is the predicted response, b_0 is the constant, b_1, b_2, and b_3 are linear coefficients and

Table 3
Coded and actual values of CCD with actual and predicted response for head and power

Trial	Coded value			Actual value			Response		Response	
	A	*B*	*C*	Imp. Eye Dia.	Vane angle	Width	Actual		Predicted	
							Head (m)	Power (W)	Head (m)	Power (W)
1	−1	−1	−1	26	37.5	4	41.14	416.63	41.06	417.12
2	1	1	−1	28	48.5	4	42.51	420.19	42.47	421.06
3	1	−1	1	28	37.5	5	41.63	427.08	41.57	427.93
4	−1	1	1	26	48.5	5	41.65	422.81	41.56	423.72
5*	0	0	0	27	43	4.5	42.23	429.73	42.25	429.52
6*	0	0	0	27	43	4.5	42.23	429.73	42.25	429.52
7	1	−1	−1	28	37.5	4	41.77	428.99	41.63	429.99
8	−1	1	−1	26	48.5	4	41.21	430.41	41.10	431.24
9	−1	−1	1	26	37.5	5	42.14	410.69	42.00	411.48
10	1	1	1	28	48.5	5	42.01	425.57	41.96	426.50
11*	0	0	0	27	43	4.5	42.23	429.73	42.25	429.52
12*	0	0	0	27	43	4.5	42.23	429.73	42.25	429.52
13	−2	0	0	25	43	4.5	41.94	417.16	42.12	416.18
14	2	0	0	29	43	4.5	43.01	423.50	43.06	422.45
15	0	−2	0	27	32	4.5	41.56	422.84	41.69	422.11
16	0	2	0	27	54	4.5	42.05	426.34	42.10	425.41
17	0	0	−2	27	43	3.5	39.66	432.17	39.75	431.41
18	0	0	2	27	43	5.5	40.07	422.73	40.15	421.83
19*	0	0	0	27	43	4.5	42.23	429.73	42.25	429.52
20*	0	0	0	27	43	4.5	42.23	429.73	42.25	429.52

Note: * centre points in CCD.

Table 4
Estimated regression coefficients for head and power

Variables	Head		Power	
Term	Coefficient	p-value	Coefficient	p-value
Constant	42.2520	0.000	429.523	0.000
A	0.4728	0.000	3.134	0.000
B	0.2063	0.007	1.650	0.011
C	0.2008	0.009	−4.792	0.000
$A \times A$	0.3433	0.004	−10.204	0.000
$B \times B$	−0.3555	0.004	−5.757	0.000
$C \times C$	−2.2954	0.000	−2.896	0.006
$A \times B$	0.8215	0.000	−13.662	0.000
$A \times C$	−0.9823	0.000	12.961	0.000
$B \times C$	−0.4521	0.028	7.510	0.001
R^2	98.73%		98.23%	
R^2 (Adj)	97.58%		96.63%	

b_{11}, b_{22}, and b_{33} are interaction coefficients and A, B, and C are control factors. The values of response, coded values, and actual values are given in Table 3. The values of the coefficients have been obtained by regression analysis with the help of Eq. (7) for the head and power.

$$\text{Head}\,(H) = 42.252 + (0.472 \times A) + (0.206 \times B) + (0.20 \times C) + (0.343 \times A^2) - (0.355 \times B^2) - (2.295 \times C^2) + (0.821 \times A \times B) - (0.982 \times A \times C) - (0.452 \times B \times C) \quad (8)$$

$$\text{Power}\,(P) = 429.523 + (3.134 \times A) + (1.65 \times B) - (4.792 \times C) - (10.204 \times A^2) - (5.757 \times B^2) - (2.896 \times C^2) - (13.663 \times A \times B) - (12.961 \times A \times C) - (7.51 \times B \times C) \quad (9)$$

The higher coefficient obtained from the regression analysis shows the significance of control parameters for the maximum head and minimum power consumption in Table 4.

To diagnose nonlinearity or nonconstant error variance, the residual plot is commonly used and is also used to find outliers. Figs. 7 and 8 show the normal probability plot of residuals, histogram of residuals, residuals vs. fits and residuals vs. order for head and power. Histogram of residuals shows the general individuality of the data of distinctive values, difference, abnormal values, and shape. Normal probability plot of residuals shows that the points commonly outline the straight line if the residuals are

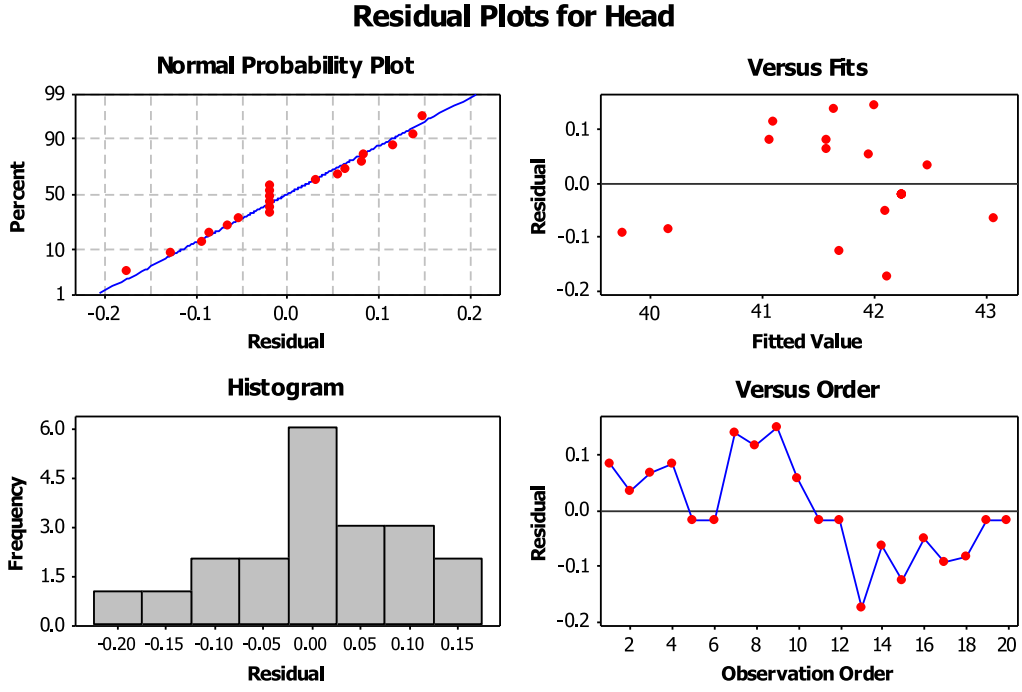

Fig. 7. Normal probability plot of residuals, vs. fits of fitted value, histogram of residual and vs. order of observation for head.

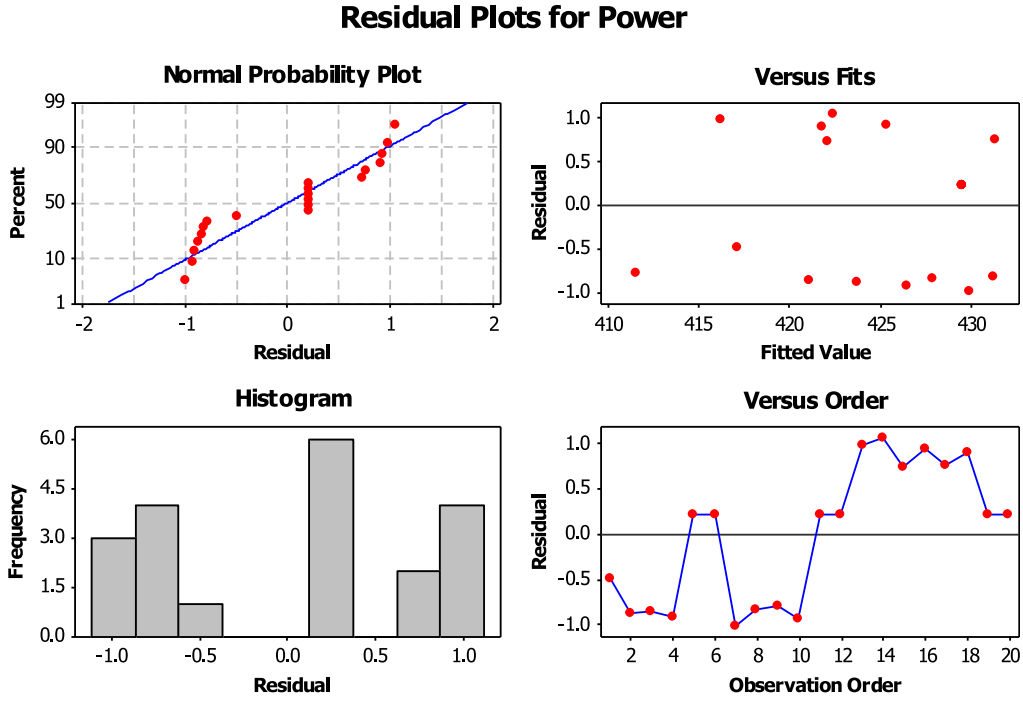

Fig. 8. Normal probability plot of residuals, vs. fits of fitted value, histogram of residual and vs. order of observation for power.

normally distributed. Residuals vs. fits show the random sample of residuals on mutual sides. Residuals vs. order of all residuals plot is used to find nonrandom error, especially of time-related effects.

The contour and surface plots for head and power are shown in Figs. 9 and 10, respectively; it is the visual display of the response surface of the fitted model. The plots were estimated from the quadratic model. The head range is fixed between 39 and 43 m, whereas the power range is fixed between 400 and 430 W for locating the optimal responses in the modified pump impeller. The hold values were given for impeller eye diameter as 27 mm, vane exit angle as 43˚C, and width of the blade at exit as 4.5 mm for the corresponding responses.

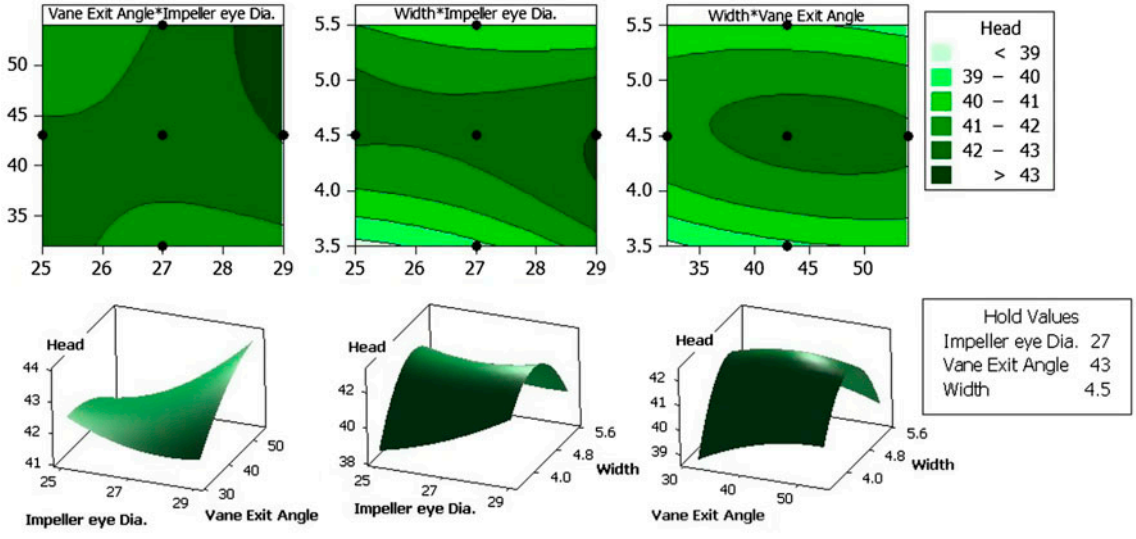

Fig. 9. Contour and surface plots of head for the vane exit angle, impeller eye diameter, and width at exit.

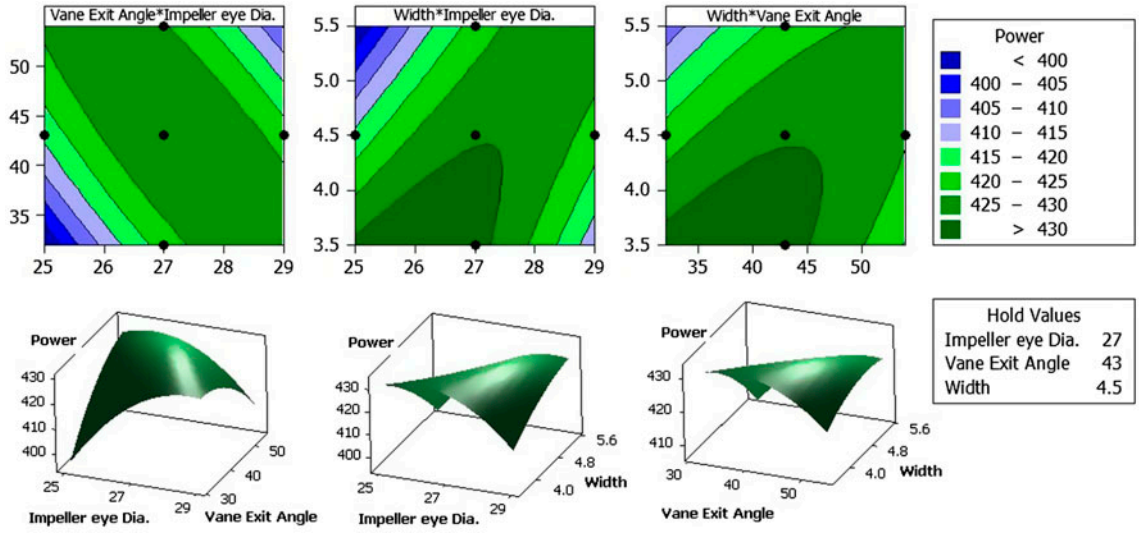

Fig. 10. Contour and surface plots of power for the vane exit angle, impeller eye diameter, and width at exit.

4. Concluding remarks

This paper explored the possibility for the improvement of the performance of a centrifugal pump impeller by means of the RSM complemented with CFD simulations. In particular, the impeller eye diameter, vane exit angle, and width of the impeller blade at exit are varied between certain ranges (Table 2) to evaluate the responses (Head and Power) using RSM. CFD analysis were performed for the coded values in CCD (Table 3) and the responses measured from CFD analysis were used to obtain the pump geometry that yield better performance via response/contour plots (Figs. 7–10).

The optimized impeller geometric parameters were numerically computed and the same were experimentally verified. CFD simulations were performed with assumptions like incompressible flow; steady state flow but viscous fluid with the rotor zone treated as moving frame (rotating turbine wheel zone); smooth walls with no-slip and standard K–ε turbulence model as boundary conditions. The following conclusions were arrived from the analysis:

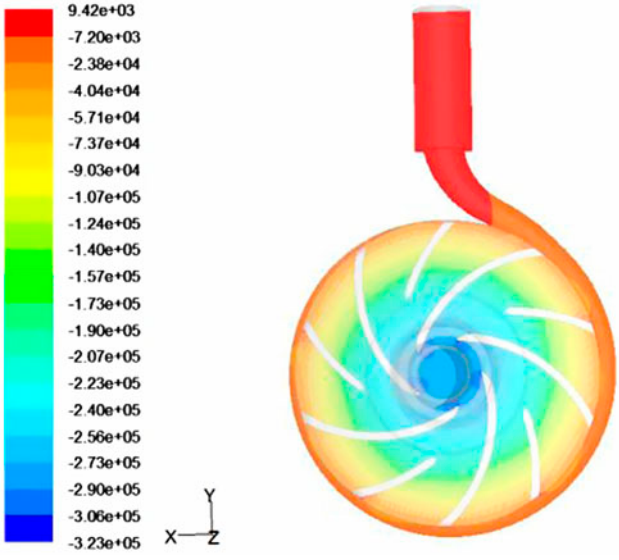

Fig. 11. Static pressure contour.

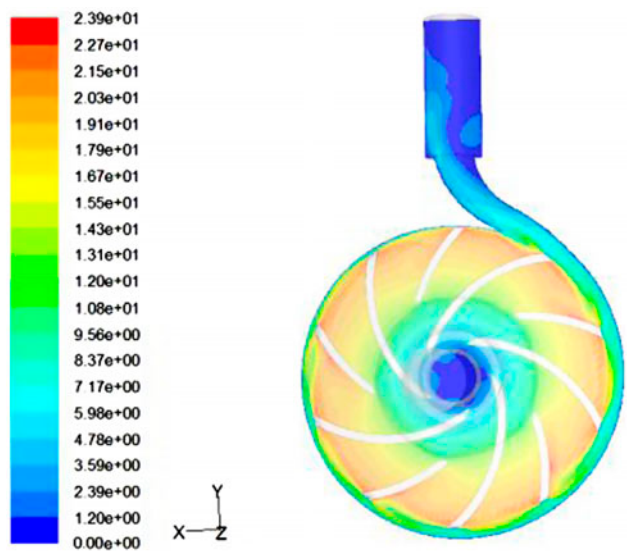

Fig. 12. Velocity contour.

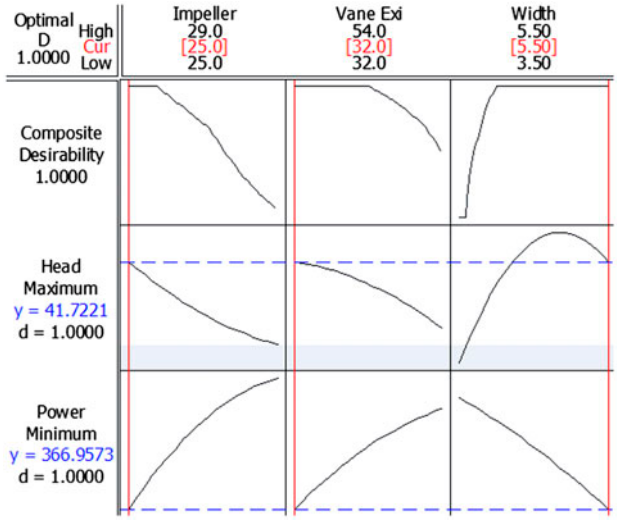

Fig. 13. Optimization plot for head and power using RSM.

- The base line pump impeller geometry dimensions were eye diameter (27 mm), vane exit angle (43˚), and width of the blade at exit (3.5 mm) offered Head (39.66 m) and power (432.17 W) at best efficiency point.
- It is obvious from the static pressure contour (Fig. 11) and velocity contour (Fig. 12), The optimized impeller geometry viz., impeller eye diameter (25 mm), vane exit angle (32˚), and width of the blade at exit (5.5 mm) which capitulates 41.72 m Head and 366.95 W Power. These results were obtained from the RSM analyses (Fig. 13).
- It is evident from Fig. 13 that the impeller eye diameter and blade angle decreased with increase in blade width for the improvement in head from 39.66 m to 41.72 m and the power consumption is decreased from 432.17 to 366.95 W.
- The volute parameters can also be taken up for enhancing the performance of centrifugal pump in future for further investigation.

Acknowledgment

The authors are immensely thankful to H. VIPIN KUMAR, Deputy Manager (Product Development) of V-Guard Industries (P) Ltd, Cochin, INDIA for providing the technical expertise and professional skills in CFD analysis to do the analysis and investigation for successfully completing the research study.

Nomenclature

RSM	—	response surface methodology
CFD	—	computational fluid dynamics
BEP	—	best efficiency point
CCD	—	central composite design
DOE	—	design of experiments
H	—	head, m
p	—	pressure, N/m^2
ρ	—	density, kg/m3
g	—	acceleration due to gravity, m/sec^2
N	—	speed, rpm
A	—	impeller eye diameter, mm
B	—	vane exit angle, ˚
C	—	width of the blade at exit, mm

References

[1] J.H. Kim, K.Y. Kim, Analysis and optimization of a vaned diffuser in a mixed flow pump to improve hydrodynamic performance, J. Fluids Eng. 134(7) (2012) 1–10.
[2] M.H. Shojaeefard, M. Tahani, M.B. Ehghaghi, M.A. Fallahian, M. Beglari, Numerical study of the effects of some geometric characteristics of a centrifugal pump impeller that pumps a viscous fluid, Comput. Fluids 60 (2012) 61–70.
[3] S.S. Yang, S. Derakhshan, F.Y. Kong, Theoretical, numerical and experimental prediction of pump as turbine performance, Renewable Energy 48 (2012) 507–513.
[4] B. Jafarzadeh, A. Hajari, M.M. Alishahi, M.H. Akbari, The flow simulation of a low-specific-speed high-speed centrifugal pump, Appl. Math. Model. 35 (2012) 242–249.
[5] R. Barrio, J. Parrondo, E. Blanco, Numerical analysis of the unsteady flow in the near-tongue region in a volute-type centrifugal pump for different operating points, Comput. Fluids 39 (2010) 859–870.
[6] J.S. Anagnostopoulos, A fast numerical method for flow analysis and blade design in centrifugal pump impellers, Comput. Fluids 38 (2009) 284–289.
[7] J. Jin, Y. Fan, W. Han, J. Hu, Design and analysis on hydraulic model of the ultra – low specific-speed centrifugal pump, International Conference on Advances in Computational Modeling and Simulation (2012) 110–114.
[8] Q. Thai, C. Lee, The cavitation behavior with short length blades in centrifugal pump, J. Mech. Sci. Technol. 24(10) (2010) 2007–2016.
[9] J. Fan, J. Eves, H.M. Thompson, V.V. Toropov, N. Kapur, D. Copley, A. Mincher, Computational fluid dynamic analysis and design optimization of jet pumps, Comput. Fluids 46 (2011) 212–217.
[10] R. Barrio, J. Fernández, E. Blanco, J. Parrondo, Estimation of radial load in centrifugal pumps using computational fluid dynamics, Eur. J. Mech. B. Fluids 30 (2012) 316–324.
[11] E.C. Bacharoudis, A.E. Filios, M.D. Mentzos, D.P. Margaris, Parametric study of a centrifugal pump impeller by varying the outlet blade angle, The Open Mechanical Eng. J. 2 (2008) 75–83.
[12] J.H. Kim, K.T. Oh, K.B. Pyun, C.K. Kim, Y.S. Choi, J.Y. Yoon, Design optimization of a centrifugal pump impeller and volute using computational fluid dynamics, IOP Conf. Ser. Earth Environ. Sci. 15(3) (2012) 1–9.
[13] J.F. Wang, J. Piechna, N. Müller, A novel design of composite water turbine using CFD, J. Hydrodyn. 24(1) (2012) 11–16.
[14] J.F. Wang, N. Müller, Numerical investigation on composite material marine current turbine using CFD, Central Europ. J. Eng. 1(4) (2011) 334–340.
[15] R. Ragothsingh, M. Nataraj, Parametric study and optimization of pump impeller by varying the design parameter using computational fluid dynamics, Int. Rev. Mech. Eng. 6 (2012) 1581–1585.
[16] M. Nataraj, V.P. Arunachalm, Optimizing impeller geometry for performance of centrifugal pump using Taquchi quality concept, Proc. Instn. Mech. Engrs, Part A, J. of Power Energy, 220(A7) (2006) 765–782.

[17] A. Papierski, A. Błaszczyk, Multiobjective optimization of the semi-open impeller in a centrifugal pump by a multilevel method, J. Theor. Appl. Mech. 49 (2011) 327–341.
[18] I.H. Cho, K.D. Zoh, Photocatalytic degradation of azo dye (Reactive Red 120) in TiO2/UV system: Optimization and modeling using a response surface methodology (RSM) based on the central composite design, Dyes Pigm. 75 (2007) 533–543.
[19] M. Bashiri, A. Farshbaf Geranmayeh, Tuning the parameters of an artificial neural network using central composite design and genetic algorithm, Scientia Iranica Transactions E: Industrial Eng. 18(6) (2011) 1600–1608.
[20] K.M. Srinivasan, Rotodynamic pumps (centrifugal and axial), New Age International (p) Ltd, New Delhi, 2008.